

LOW-TEMPERATURE MOBILITY BEHAVIOUR IN SUBMICRON MOSFETS AND RELATED DETERMINATION OF CHANNEL LENGTH AND SERIES RESISTANCE

CH. NGUYEN-DUC, S. CRISTOLOVEANU and G. GHIBAUDO

Laboratoire de Physique des Composants à Semiconducteurs, UA-CNRS 840, ENSER-INPG,
23 Av des Martyrs, 38031 Grenoble, France

(Received 29 January 1986; in revised form 6 May 1986)

Abstract—The electron mobility behaviour in submicron MOSFETs is studied in the temperature range of 77–300 K. As the effective channel length is reduced, the effective mobility as well as the field-effect mobility are found to decrease and to become less temperature dependent. These experimental results are explained by the influence of series resistance and effective channel length, which are both temperature dependent. The possibility of accurate determination of series resistance and “pure” mobility is demonstrated. A new method is proposed to determine submicron MOSFET channel length at low temperatures.

NOTATION

G_{gm}	maximum transconductance	n_i	intrinsic electron density
W	gate width	Φ_{Fn}	electron Fermi potential referred to mid-gap
L_m	gate length	Φ_{Fp}	hole Fermi potential referred to mid-gap
L_{eff}	effective channel length	E_a	acceptor energy
I_d	drain current	E_{Fp}	substrate Fermi energy
V_d	drain voltage	E_{Fn}	drain Fermi energy
V_g	gate voltage	Y_s	source lateral depletion width
V_b	substrate voltage	Y_d	drain lateral depletion width
N_{inv}	inversion charge density	Ψ_s	surface potential
Q_{inv}	inversion charge	μ_{max}	maximum field-effect mobility
q	electron charge		
μ_{eff}	effective mobility		
G_d	effective channel conductance		
G_d^0	intrinsic channel conductance		
R_d	source-drain series resistance		
μ_{eff}^0	intrinsic effective mobility		
G_g	device transconductance		
G_g^0	intrinsic transconductance		
μ_{FE}	field-effect mobility		
μ_{FE}^0	intrinsic field-effect mobility		
μ_0	“pure” mobility		
N_c	critical charge density		
C_{ox}	gate oxide capacitance		
V_t	inversion charge threshold voltage		
θ	intrinsic mobility reduction factor		
θ^*	mobility reduction factor		
R_c	contact resistance		
R_j	diffusion sheet resistance		
R_{sp}	spreading resistance		
x_j	source and drain junction depth		
x_c	channel thickness		
k	Boltzmann's constant		
T	temperature in degrees Kelvin		
F_s	surface electric field		
N_{depl}	surface depletion charge density		
ϵ_{si}	permittivity of the silicon		
Δ_L	channel length reduction		
Y_m	gate-source and gate-drain overlap		
W_s	source depletion width		
W_d	drain depletion width		
N_A	channel doping		
N_A^-	ionized acceptor concentration		
V_{bi}	junction built-in voltage		
N_D^+	source and drain ionized donor concentration		

1. INTRODUCTION

Up to now all the methods used to determine the MOSFET parameters (effective channel length, series resistances, etc . . .) were based on the hypothesis of a carrier mobility which is independent of the transistor channel length[1–5]. This hypothesis is valid only for long transistors and temperatures around 300 K. It has been shown that with reduction of the dimensions of MOSFETs, the mobility becomes dependent on the channel length[6–8]. In addition, the low-temperature dependence of the transconductance[9] or mobility[6] is different in long and short devices. For example, at 77 K the transconductance “gain” G_{gm} (77 K)/ G_{gm} (294 K) was found to be 1.47 for $L_m = 0.8 \mu\text{m}$ and 7.46 for $L_m = 50 \mu\text{m}$ device[9]. In other words, the assumptions used in traditional methods are no longer exact and must be reconsidered for very-short-channel MOSFETs and at low temperatures, accurate channel-length determination being essential for device analysis and process control in MOS-VLSI technology.

In this paper, we first report the experimental variations of the MOSFET mobility as a function of channel length and temperature; distinction will be made between the intrinsic effective and field-effect mobilities. The results will be explained by the influence of series resistance and effective channel

length, both of which are temperature dependent. Different components of the series resistance will be studied and a method will be proposed to deduce, for each temperature and transistor, the total resistance value as well as the intrinsic mobility. Another method will be also proposed for the determination of the effective channel length in the temperature range of 77–300 K. Finally, the rough experimental mobility data will be analysed by a more realistic model taking into account the channel-length correction.

2. EXPERIMENTAL CONDITIONS

The experiments were carried out on the MOSFETs with poly-Si gate width $W = 8.8 \mu\text{m}$ and length from $L_m = 0.5 \mu\text{m}$ to $L_m = 5 \mu\text{m}$ fabricated at the LETI Laboratories in Grenoble. The gate oxide was 125 Å thick, the depth of source and drain junctions was $0.17 \mu\text{m}$, and channel boron double implantation was realized in the *p*-type substrate ($2 \times 10^{15} \text{ cm}^{-3}$) to give surface doping of approximately $1 \times 10^{17} \text{ cm}^{-3}$.

The linear region of the family of I_d vs V_d curves with V_g as a parameter was used to extract the effective electron mobility as a function of the gate voltage (or inversion channel charge). From I_d vs V_g curves the threshold voltage, transconductance and field-effect mobility were determined. The mobility data reported in this paper correspond to the ohmic range of V_d of 0–50 mV. The measurements were performed with the help of HP4140B computer-driven system, in a cryostat controlled by OXFORD-3120 Temperature Controller.

3. RESULTS

The characteristics $G_{gm}(T)/G_{gm}(300 \text{ K})$ vs temperature of our samples (Fig. 1) show that when the

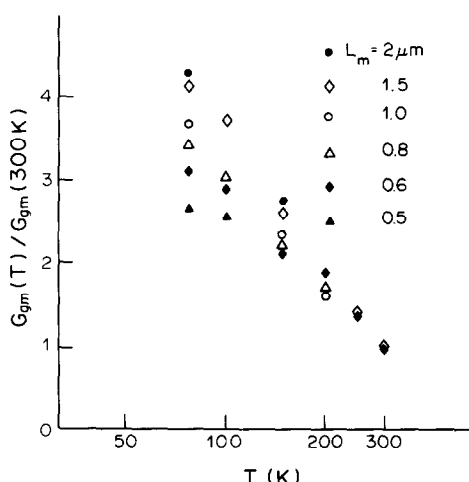


Fig. 1. Experimental variation of the normalized maximum transconductance with temperature for several channel lengths ($N_A = 10^{17} \text{ cm}^{-3}$).

channel length is reduced, the electron mobility decreases and its temperature dependence is modified. Similar features have been previously observed on lower doped MOSFETs[6]. Various models have been proposed to explain the channel length and temperature dependence of the mobility of MOSFETs. As devices are scaled down, second-order effects, such as velocity saturation[10], increased source and drain resistance[11], quasi-ballistic transport[6], threshold voltage variation[12] and hot electron effects[13], can cause the transconductance, or mobility, to deviate from theoretical expectations. Increased series resistance[9] and “effective” oxide charge density (“edge effect”)[6] have been also invoked to explain the mobility reduction in small-size MOSFETs at low temperature.

Because of the important role of series resistance in the electron mobility evolution of micron and sub-micron MOSFETs[7,11,14] we shall mainly consider this effect.

3.1 Transconductance and mobility

MOSFET drain current in the ohmic region is given by

$$I_d = \frac{W}{L_{\text{eff}}} q N_{\text{inv}} \mu_{\text{eff}} V_d, \quad (1)$$

where I_d , V_d are drain current and voltage, W is channel width, L_{eff} its effective length, N_{inv} is the channel electron density, q electron charge and μ_{eff} effective electron mobility. The effective channel conductance is thus expressed by

$$G_d = \frac{W}{L_{\text{eff}}} q N_{\text{inv}} \mu_{\text{eff}}. \quad (2)$$

On the other hand, the total effective conductance G_d due to the intrinsic channel conductance G_d^0 and the total source-drain series resistance R_{sd} is given by[7]

$$G_d(V_g) = \frac{G_d^0(V_g)}{(1 + R_{sd} G_d^0)}, \quad (3)$$

where

$$G_d^0 = \frac{W}{L_{\text{eff}}} q N_{\text{inv}} \mu_{\text{eff}}^0 \quad (4)$$

and μ_{eff}^0 is the intrinsic effective mobility.

The device transconductance $G_g(V_g) = \delta G_d / \delta V_g$ becomes[7]

$$G_g(V_g) = \frac{G_d^0(V_g)}{(1 + R_{sd} G_d^0)^2}, \quad (5)$$

where $G_g^0(V_g) = \delta G_d^0 / \delta V_g$ is the intrinsic transconductance associated with the channel conductance $G_d^0(V_g)$.

Equations (2)–(4) give

$$\mu_{\text{eff}} = \frac{\mu_{\text{eff}}^0}{(1 + R_{sd} G_d^0)} = \frac{\mu_{\text{eff}}^0}{\left(1 + R_{sd} \frac{W}{L_{\text{eff}}} q N_{\text{inv}} \mu_{\text{eff}}^0\right)}. \quad (6)$$

We obtain from (4) and (5) the field-effect mobility

$$\mu_{FE} = \frac{\mu_0^0}{(1 + R_{sd}G_d^0)^2} = \frac{\mu_0^0}{\left(1 + R_{sd} \frac{W}{L_{eff}} qN_{inv} \mu_{eff}^0\right)^2}, \quad (7)$$

where μ_{FE}^0 is the intrinsic field-effect mobility. Equations (6) and (7) clearly show that the effective mobility and field-effect mobility are differently affected by the presence of series resistance. They also show that the shorter the channel length, the more important becomes the role of series resistance. Moreover, for the same MOSFET and at the same conditions, the field-effect mobility is always smaller than the effective mobility, as was experimentally found by Sun and Plummer[15].

Now, if we take into account the mobility reduction with the increasing inversion charge, we have[16]

$$\mu_{eff}^0 = \frac{\mu_0}{1 + N_{inv}/N_c}, \quad (8)$$

where μ_0 is the "pure" mobility, function of the scattering processes, and N_c is the critical charge involving the mobility decrease ($N_c \simeq 1-2 \times 10^{13} \text{ cm}^{-2}$). In strong inversion, when $Q_{inv} = C_{ox}(V_g - V_t)$, eqn (8) reduces to the conventional relation

$$\mu_{eff}^0 = \frac{\mu_0}{1 + \theta(V_g - V_t)}, \quad (9)$$

where C_{ox} is the gate oxide capacitance, V_t the temperature-dependent inversion charge threshold voltage, and θ is the mobility reduction factor $\theta = C_{ox}/qN_c$.

Incorporation of (8) into (6) yields

$$\mu_{eff} = \frac{\mu_0}{\left(1 + N_{inv}/N_c + R_{sd} \frac{W}{L_{eff}} qN_{inv} \mu_0\right)}. \quad (10)$$

Equation (10) will be used later in analysing experimental mobility data.

In summary, there are several definitions of the mobility concept in MOSFETs. The field-effect mobility (μ_{FE}^0) and the effective mobility (μ_{eff}^0) are well defined for "long" MOSFETs where $R_{sd}G_d^0 \ll 1$. In the "short" devices, series resistances alter the real mobility values so that μ_{FE} and μ_{eff} have to be calculated using eqns (7) and (10), respectively. The "pure" mobility μ_0 is really independent of series resistance and is directly dependent on the genuine scattering process in the channel. Moreover, the mobility reduction factor θ^* of μ_{eff} is simply related to the intrinsic mobility reduction factor θ by the linear relationship $\theta^* = \theta + C_{ox}R_{sd}W\mu_0/L_{eff}$.

3.2 Series resistances

The major components of the series resistance R_{sd} are: (1) the contact resistance R_c , resulting from both the aluminium line resistance and the finite contact resistivity between the metal and the doped semiconductor; (2) the diffusion sheet resistance of source and

drain regions R_j ; and (3) the spreading (or injection) resistance R_{sp} , due to the crowding of the current-flow lines in the vicinity of the channel[17]. Therefore

$$R_{sd} = R_c + R_j + R_{sp}. \quad (11)$$

Both the contact and diffusion resistances were found to decrease with decreasing temperature[18]. With regard to the spreading resistance, Baccarani and Sal-Halasz have derived an analytical expression[17]

$$R_{sp} = \frac{2}{\Pi} \frac{R_j x_j}{W} \ln\left(0.75 \frac{x_j}{x_c}\right), \quad (12)$$

where x_j is the source and drain junction depth, x_c the channel thickness. We use the process parameters $x_j = 0.17 \mu\text{m}$, $W = 8.8 \mu\text{m}$, $R_j = 60 \Omega$ at 300 K and the classical approximation for x_c [19]

$$x_c = \frac{kT}{qF_s}, \quad (13)$$

where $F_s = q(N_{depl} + N_{inv})/\epsilon_{Si}$ is the surface electric field. The calculated spreading resistance of our devices is shown in Fig. 2, as a function of gate voltage, V_g . The influence of the temperature and substrate voltage, V_b , is emphasized for the first time. The decrease in R_{sp} with decreasing temperature results from the fact that the sheet resistance of the source R_j is reduced when the temperature is lowered[18]. Furthermore, the dependence of spreading resistance on gate voltage and substrate voltage is relatively weak. Its value is between 3 and 4.5 Ω (normalized values being 26 and 39 $\Omega \mu\text{m}$, respectively), in the voltage range of practical interest, and is much smaller than other components of R_{sd} . In conclusion, the total series resistance R_{sd} will decrease when the temperature is lowered.

3.3 Experimental data

In Fig. 3 we plot the effective mobility versus inversion channel charge for a 3- μm -long MOSFET at different temperatures. The discrete points represent the effective mobility obtained by measuring the conductance and using eqn (2), where the inversion charge is determined as $Q_{inv} = C_{ox}(V_g - V_t)$ and L_{eff} is obtained as in Section 4. A good fitting (solid lines) is obtained by exploiting eqn (10) and only two adjustable parameters (R_{sd} and μ_0) for each curve. These parameters listed in Table 1 are determined with an accuracy of 5%. Table 1 clearly demonstrates that series resistance monotonically decreases, while the pure mobility μ_0 increases with decreasing temperature. The difference between the experimental points and the calculated curves at relatively low inversion charge density is attributed to the proximity of weak inversion regime, where the previous calculations are less accurate and where potential fluctuations (caused by randomly distributed charges at Si-SiO₂ interface) may also occur, essentially at low temperature[20-22]. As we are in strong and intermediate inversion the value of μ_{FE}^0 is approxi-

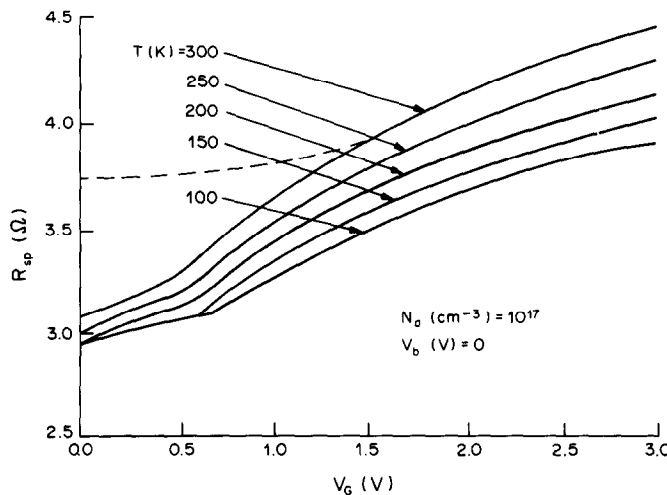


Fig. 2. Spreading resistance vs gate voltage for different temperatures at $V_b = 0$. Dotted line shows R_{sp} for $V_b = -3$ V at 300 K.

mately equal to μ_{eff}^0 [16]. So, using the values of R_{sd} and μ_0 we can calculate μ_{eff} and μ_{FE} for any channel length and temperature. Room temperature mobility variations vs inversion charge are plotted in Fig. 4, with the effective channel length as a further parameter. The mobility decrease is seen to be more accentuated in short devices, as the mobility reduction factor θ^* is higher than θ .

The normalized effective mobility vs temperature is presented in Fig. 5(a) for the range 77–300 K with the length as a parameter. The inversion channel charge Q_{inv} used for the calculations was taken to be of $1.6 \times 10^{-7} \text{ C} \cdot \text{cm}^{-2}$ ($N_{inv} = 10^{12} \text{ cm}^{-2}$), which corresponds to the value where the electron mobility experimentally reaches its maximum. This figure clearly shows that the mobility variation with temperature is strongly correlated with the channel length: for a MOSFET of $2.85 \mu\text{m}$ long, μ_{eff} increases with decrease of temperature by a factor of 5.3, while

for a $0.35\text{-}\mu\text{m}$ MOSFET this factor is only 3.4. It is clear that similar curves plotted for a higher gate voltage (inversion charge) show an attenuated temperature variation, since the denominator of eqn (10) increases.

In Fig. 5(b) are given the corresponding variations of the field-effect mobility which also include the effect of series resistance and exhibit a very good agreement with the experimental results of Fig. 1: the field-effect mobility increases more slowly than the effective mobility at low temperature and tends to become temperature invariant for very short devices. Note that the pure mobility shows a temperature variation in good agreement with experimental data obtained for long MOSFETs. Furthermore, Fig. 6 gives the normalized electron mobility vs the effective channel length for $T = 300$ K and 77 K; it illustrates that the mobility variation with length is more significant at low temperature and, therefore, allows explaining the experimental results previously reported[6,8]. Thus, the conclusion is that, the decrease in R_{sd} with decreasing temperature is offset by the more important increase in μ_0 [eqn (10) and Table 1], which causes the global influence of series resistances to be more pronounced at low temperatures. This influence is enhanced in short-channel MOSFETs and results in a much smaller mobility gain.

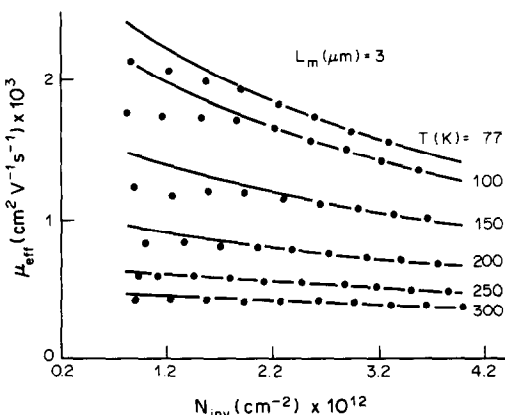


Fig. 3. Effective mobility vs inversion channel charge for 3- μm MOSFET with temperature as parameter: ●, experiments; —, theoretical fitting using (10).

Table 1. Fitting parameters for effective mobility calculations of 3- μm -long MOSFET

T (K)	R_{sd} (Ω)	μ_0 ($\text{cm}^2/\text{V sec}$)
300	135	515
250	130	700
200	125	1050
150	120	1700
100	115	2600
77	110	3000

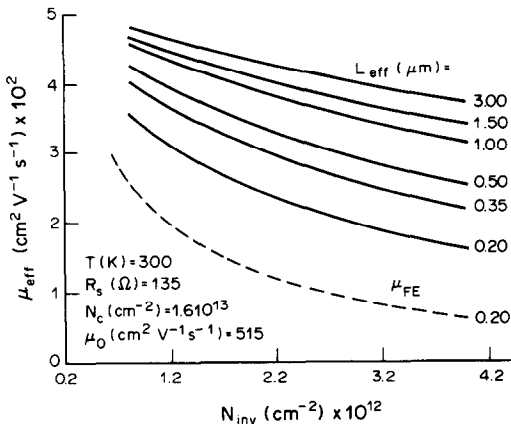
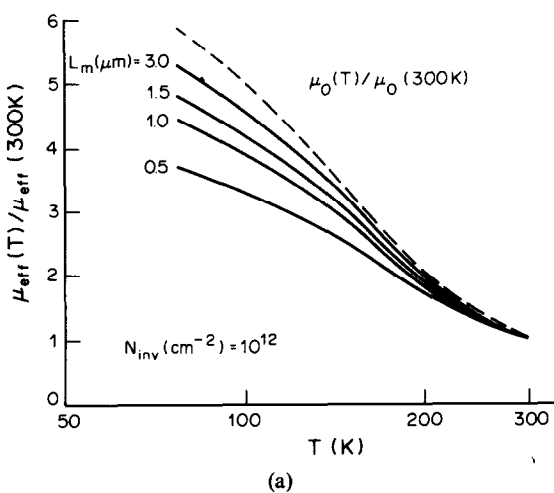
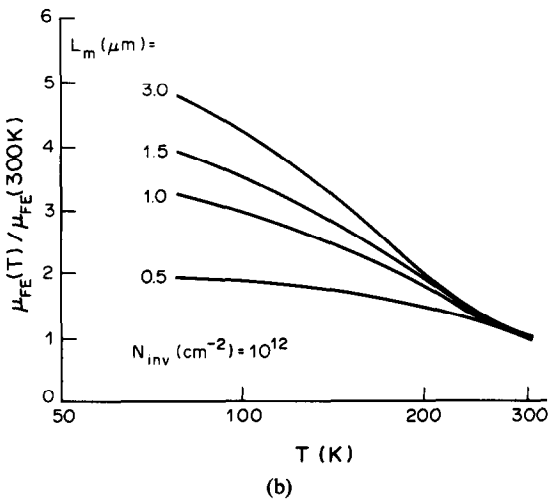


Fig. 4. Theoretical variation of the effective mobility vs inversion channel charge for several channel lengths at 300 K. Parameters: $R_s = 135 \Omega$, $\mu_0 = 515 \text{ cm}^2/\text{V sec}$, $N_c = 1.6 \times 10^{13} \text{ cm}^{-2}$. The dotted line shows the field-effect mobility variation.



(a)



(b)

Fig. 5. Theoretical variation of the normalized effective mobility (a) and field-effect mobility (b) against temperature for several channel lengths ($N_{\text{inv}} = 1 \times 10^{12} \text{ cm}^{-2}$). The dotted line in (a) shows the pure mobility variation.

4. DETERMINATION OF THE EFFECTIVE CHANNEL LENGTH

Once it is established that the mobility depends on the channel length even for relatively "long" MOSFETs, the methods of determination of L_{eff} , usually based on the hypothesis of constant mobility, must be corrected. For example, the use of such methods[4,5] sometimes gives even negative values of ΔL (channel length reduction) below 150 K. Here, we propose a method which allows a more realistic and precise determination of submicron MOSFET channel length at low temperatures.

Let us consider the cross-section of a MOSFET shown in Fig. 7[23], where L_m is the gate length, Y_m the gate-source and gate-drain overlap (technological factor), W_s and W_d are the depletion widths of the source and drain. For a one-dimensional abrupt junction, W_s and W_d are defined as[10]

$$W_d = \left[\frac{2\epsilon_{\text{Si}}}{qN_A} \left(V_{bi} + V_d - \frac{2kT}{q} \right) \right]^{1/2} \quad (14)$$

and $W_s = W_d(V_d = 0)$.

V_{bi} is the built-in voltage of the junction

$$V_{bi} = |\Phi_{Fn}| + \Phi_{Fp} \simeq \frac{kT}{q} \ln \left(\frac{N_A^- N_D^+}{n_i^2} \right), \quad (15)$$

where Φ_{Fn} and Φ_{Fp} are Fermi potentials of n - and p -side (referred to the mid-gap), respectively, N_A the channel doping, N_D^+ the source and drain ionized impurity concentration, and n_i is the intrinsic carrier concentration. As the temperature is lowered, the number of ionized acceptors N_A^- is obtained by[18]

$$N_A^-(T) = \frac{N_A}{1 + 4 \exp \left(\frac{E_a - E_{Fp}}{kT} \right)}. \quad (16)$$

where E_a ($\simeq 0.045$ eV) is the acceptor energy. The substrate Fermi energy E_{Fp} moves at low temperatures closer to the valence band, while the source

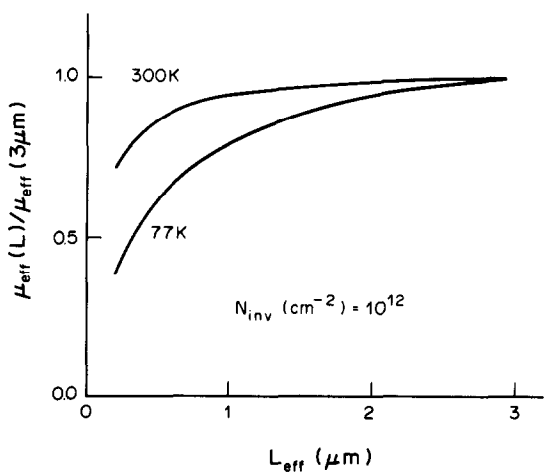


Fig. 6. Theoretical variation of the normalized effective mobility with effective channel length at 300 K and 77 K ($N_{\text{inv}} = 1 \times 10^{12} \text{ cm}^{-2}$).

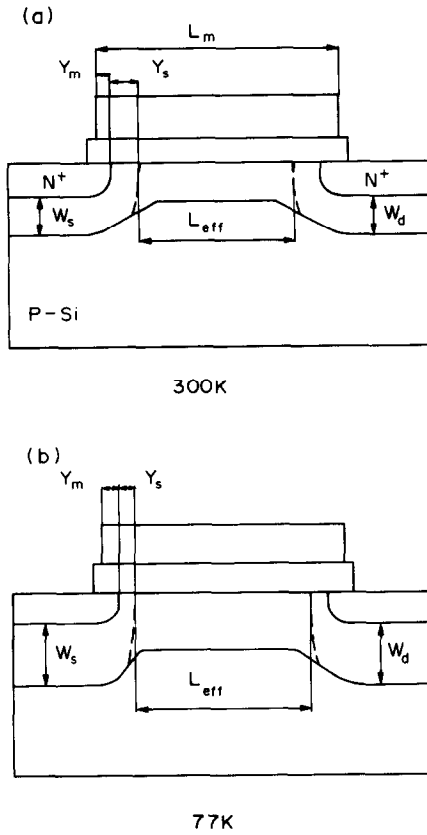


Fig. 7. Schematic representation of the MOSFET channel at (a) 300 K and (b) 77 K [23].

and drain Fermi energy E_{Fn} remains fairly constant, due to the high impurity concentration in these regions. There is, therefore, an increase in the built-in potential which makes W_s and W_d values larger at low temperatures than at 300 K. This is not the case of the lateral depletion width (Y_d or Y_s) at the inverted surface [24]

$$Y_d = \left[\frac{2\epsilon_{Si}}{qN_A} (V_{bi} + V_d - \Psi_s) \right]^{1/2}$$

$$Y_s = Y_d(V_d = 0), \quad (17)$$

which is smaller than the $p-n$ depletion width due to the surface potential Ψ_s (roughly equal to $2\Phi_{Fp}$). We see, therefore, that even though W_s increases from 300 to 77 K, corresponding Y_s decreases. Since $L_{eff} = L_m - 2Y_m - Y_s - Y_d$ and Y_m does not change with temperature, the channel length assumes a larger value at low temperature (Fig. 7). Moreover, the carrier "freeze-out" situation, at the semiconductor surface under the gate, is different from that in the bulk. The acceptors in the surface depletion region are all ionized due to the band bending [18]; the surface value of N_A at 77 K is, therefore, roughly equal to that at 300 K. Finally, for the transistors with lightly doped substrates, the effective length increase is accentuated because of the stronger variation of Fermi level with the temperature. This is

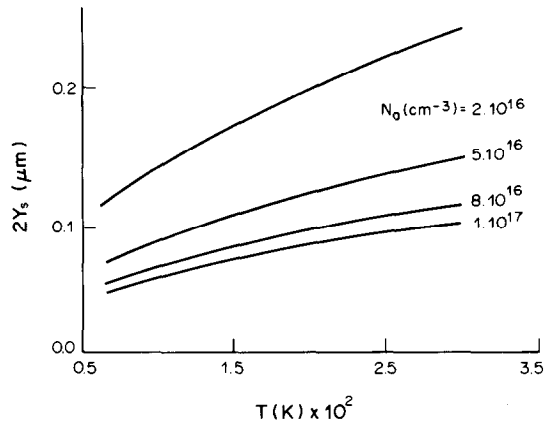


Fig. 8. Surface depletion width ($2Y_s$) vs temperature for several values of N_A .

illustrated in Fig. 8 which shows the values of $2Y_s$ ($2Y_s = Y_s + Y_d$ in equilibrium) calculated for several values of N_A , as a function of the temperature.

The procedure to determine $L_{eff}(T)$ consists, therefore, of:

- (1) determining ΔL , then L_{eff} at 300 K using one of the reported methods [1-5],
- (2) finding the gate overlap $2Y_m = \Delta L - 2Y_s$ (300 K) using Fig. 8,
- (3) obtaining corrected value $L_{eff}(T) = L_m - 2Y_m - 2Y_s(T)$.

It is clear that this increase in channel length at 77 K will cause a higher mobility to be deduced from the same conductance (or transconductance) experimental values. Thus, we can now compare

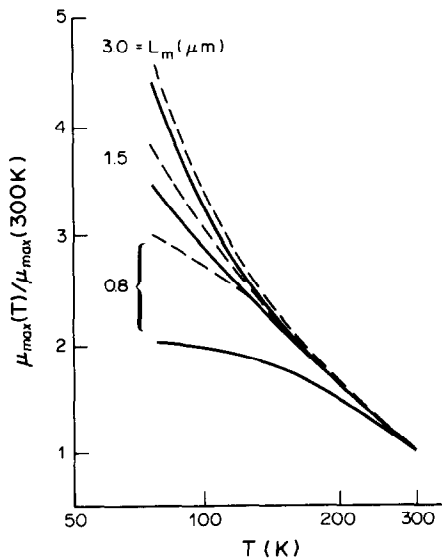


Fig. 9. Experimental variation of the normalized mobility in lower doped MOSFETs ($N_A = 2 \times 10^{16} \text{ cm}^{-3}$). Full lines are obtained from transconductance results (similar to those of Fig. 1) by considering constant effective length [6] and dotted lines are corrected curves calculated using the channel length increase at low temperature.

the mobility obtained at 77 K by supposing constant ΔL with that found when the temperature dependence of ΔL is taken into account using Fig. 8. For the MOSFETs used in our experiments ($N_A = 1 \times 10^{17} \text{ cm}^{-3}$), the difference in the effective length, and therefore in the electron mobility, between the two ways of determining L_{eff} is 1.9% for $L_m = 3 \mu\text{m}$ and 8.6% for $L_m = 0.5 \mu\text{m}$, involving small corrections in Fig. 1. In contrast, for the MOSFETs whose channel doping $N_A = 2 \times 10^{16} \text{ cm}^{-3}$, this difference is important and reaches 4 and 42.3% for $L_m = 3$ and $0.5 \mu\text{m}$, respectively. For this reason, previous experimental results[6] obtained in a similar way to those of Fig. 1 have to be reconsidered. The correction is shown in Fig. 9 and allows us to see that the precision of L_{eff} may play an important role in determining the mobility from the conductance or transductance measurements, particularly for the very-short-channel MOSFETs.

5. CONCLUSION

Experimental curves of temperature dependence of the mobility in short-channel devices have been reported. Distinction was made between the field-effect and effective mobility, which present different variations. The series resistance and the temperature dependence of the channel length were used to explain the electron mobility behaviour of micron and submicron MOSFETs as a function of channel length and temperature. As the channel length is reduced, the mobility seems to decrease and to become less influenced by the temperature. We have shown that even for relatively "long" transistors, both effective and field-effective mobilities depend on the channel length. This dependence is found to be accentuated at low temperature due to the increase in the "pure" mobility.

The possibility to accurately determine the series resistance and the pure mobility by fitting effective mobility vs inversion charge curves was demonstrated. A new method has been proposed to determine MOSFET channel length at low temperatures. The method was proven to be useful and should be

systematically used for accurate studies of very-short-channel MOSFETs at low temperatures.

Acknowledgements—The authors are grateful to LETI Laboratories, CIME Microelectronic Center (Grenoble) and GCIS organisation for supporting this work and to Miss M. Gri for her technical assistance.

REFERENCES

1. J. Chern, P. Chang, R. Motta and N. Godinho, *IEEE Electron Dev. Lett.* **EDL-1**, 170 (1980).
2. K. Peng and M. Afrimowitz, *IEEE Electron Dev. Lett.* **EDL-3**, 360 (1982).
3. F. De la Moneda, H. Cotecha and M. Shatzkes, *IEEE Electron Dev. Lett.* **EDL-3**, 10 (1982).
4. P. Rossel, H. Tranduc, J. Sanchez and A. Bellaouar, *Rev. Phys. Appl.* **18**, 487 (1983).
5. Chu-Hao, B. Cabon-Till, S. Cristoloveanu and G. Ghibaudo, *Solid-St. Electron.* **28**, 1025 (1985).
6. S. Cristoloveanu, G. Ghibaudo and Chu-Hao, *Physica* **129B**, 542 (1985).
7. B. Cabon-Till, G. Ghibaudo and S. Cristoloveanu, *Electron. Lett.* **21**, 457 (1985).
8. L. Akers, M. Holly and J. Ford, *Solid-St. Electron.* **28**, 605 (1985).
9. J. Tzou, C. Yao, R. Cheung and H. Chan, *IEEE Electron Dev. Lett.* **EDL-6**, 33 (1985).
10. S. Sze, *Physics of Semiconductor Devices*. John Wiley, New York (1981).
11. Y. El-Mansy, *IEEE Trans. Electron Dev.* **ED-29**, 567 (1982).
12. L. Akers and J. Sanchez, *Solid-St. Electron.* **25**, 621 (1981).
13. E. Takeda and N. Suzuki, *IEEE Electron Dev. Lett.* **EDL-4**, 111 (1983).
14. L. Rish, *IEEE Trans. Electron Dev.* **ED-30**, 959 (1983).
15. S. Sun and J. Plummer, *IEEE Trans. Electron Dev.* **ED-27**, 1497 (1980).
16. G. Ghibaudo, *Phys. Stat. Sol. (a)* **95**, 323 (1986).
17. G. Baccarani and G. Sai-Halazs, *IEEE Electron Dev. Lett.* **EDL-4**, 27 (1983).
18. F. Gaenslen, V. Rideout, E. Walker and J. Walker, *IEEE Trans. Electron Dev.* **ED-24**, 218 (1977).
19. F. Stern, *CRC Critical Rev. Solid-St. Sci.* **499** (1974).
20. J. Brews, *J. appl. Phys.* **46**, 2193 (1975).
21. G. Ghibaudo, Doctor-ès-sciences thesis, INP-Grenoble (1984).
22. E. Arnold, *Appl. Phys. Lett.* **25**, 705 (1974).
23. A. Kamgar, *IEEE Trans. Electron Dev.* **ED-29**, 1226 (1982).
24. G. Taylor, *IEEE Trans. Electron Dev.* **ED-25**, 337 (1978).